Optica Applicata, Vol. XXX, No. 1, 2000

Tapered rib waveguides: fast and accurate finite difference beam propagation method

SŁAWOMIR SUJECKI

National Institute of Telecommunications, ul. Szachowa 1, 04–894 Warszawa, Poland.

TREVOR M. BENSON, PHILLIP SEWELL, PETER C. KENDALL

Department of Electrical and Electronic Engineering, University of Nottingham, University Park, Nottingham NG7 2RD, UK.

A novel implementation of the finite difference beam propagation method (FD BPM) for optical rib waveguide structures in air is presented. Calculations for typical gallium arsenide based rib waveguide tapers confirm that the new approach is faster and requires less memory than previously used techniques, whilst maintaining accuracy. This is achieved by incorporating known analytical behaviour into a direct numerical algorithm.

1. Introduction

The finite difference beam propagation method (FD BPM) [1] is widely used to model optical structures of practical importance, including optical rib waveguide tapers (Fig. 1**a**) which are the focus of the studies described in this paper. When analysing such optical tapers in rectangular coordinates [2], it has been almost mandatory to model the oblique boundaries between core and cladding as a staircase approximation. New results [3]–[5] now indicate that numerical noise introduced by staircasing [3] can be substantially suppressed by the use of non-orthogonal, tapered or tapered-oblique coordinate systems (Fig. 1**b**) [4], [5] with the FD BPM. This approach allows the actual oblique boundaries between the core and cladding to be modelled correctly and proves to be faster and to require less computer memory than the standard (rectangular coordinate) FD BPM algorithm for the same accuracy [3]. Here we show that for a wide range of practically useful structures an even more efficient algorithm can be developed. The idea is based upon the observation that in air clad waveguide structures used in integrated optics, any scattered light is primarily radiated into the substrate or the outer slab and the air only supports a rapidly decaying field. Although this decaying field cannot be ignored without compromising accuracy, the *effects* of its presence are excellently approximated by slightly increasing the dimensions of the semiconductor structure by the Goos–Hänchen penetration distance and imposing a zero field boundary (Fig. 1**c**). This concept was introduced in [6] and successfully applied to decrease the memory requirement for FD mode solvers [7]; it also constitutes the backbone of

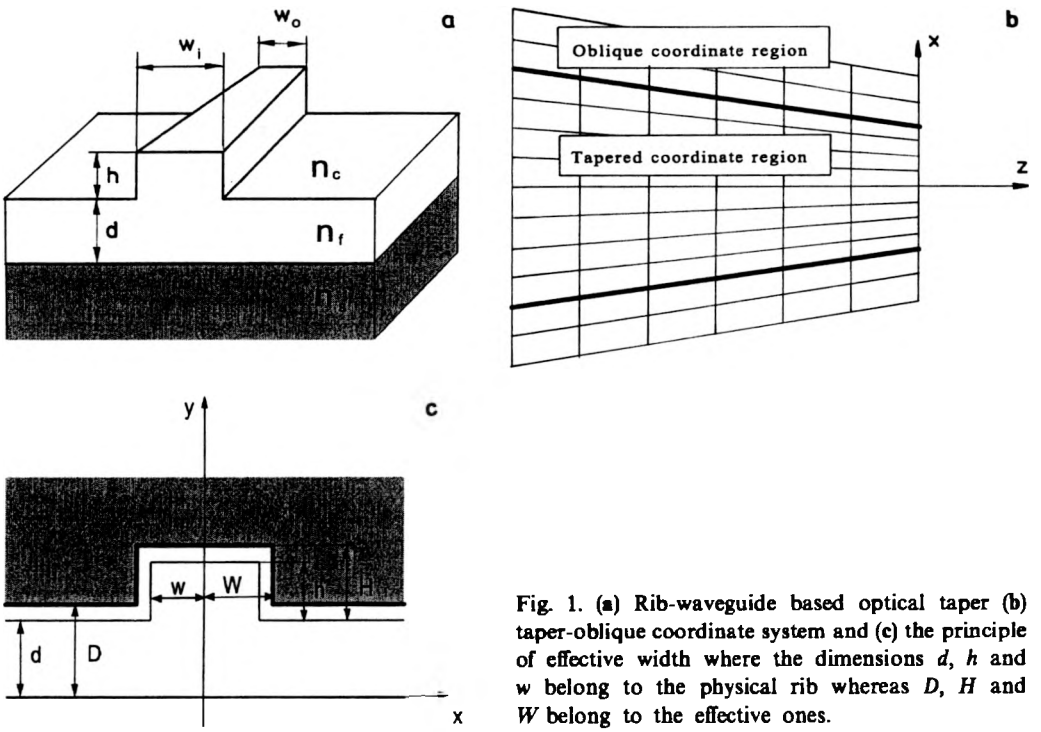

Fig. 1. (**a**) Rib-waveguide based optical taper (**b**) taper-oblique coordinate system and (**c**) the principle of effective width where the dimensions d, h and w belong to the physical rib whereas D, H and W belong to the effective ones.

the spectral index method, a very fast and accurate technique for the modal analysis of semiconductor rib waveguides in air [8].

For maximum benefit we have simultaneously applied both the ideas of non-orthogonal coordinate transforms and displaced boundaries to 3D FD BPM analysis of optical tapers. The results obatined confirm that a considerable gain in the efficiency of the FD BPM approach has been achieved, both in terms of calculation time and memory requirements, and that the considerable advantages of using the non-orthogonal coordinate algorithm are preserved.

2. Implementation

Following previously established procedures, the paraxial wave equation expressed in the tapered coordinate system is derived from the Helmholtz equation for the scalar potential and solved using the finite difference Crank–Nicolson scheme [4]. A thorough description of this may be found in [3]–[5]. The effective dimensions of the guide (Fig. 1**c**) are calculated using the relations [6]: $W = w + \delta$, $H = h + \delta$, $D = d + \delta$, where $\delta = (\beta^2 - k_c^2)$ and k_c is the wavenumber in the air cladding (Fig. 1**a**). An ILU(0) pre-conditioned Bi-CGSTAB algorithm has been used [9], [10] to solve the resulting set of the algebraic equations, with a transparent boundary condition (TBC) applied on the open boundaries of the analysis window [11].

3. Results and discussion

To demonstrate the advantages of the tapered FD BPM with displaced boundaries we have analysed propagation in a range of air-clad GaAs-based tapers with $d+h=$ 1 μm (Fig. 1**a**). In each case the waveguide is tapered from a full width of 3 μm to 1.6 μm over a distance of 100 μm, the refractive indices in the core and substrate are 3.44 and 3.40, respectively, and the operating wavelength is 1.15 μm. A symmetric taper is assumed such that only half the cross-section is considered. In the first instance the embossed rib waveguide taper (with $d=0$ and $h=1$ μm) is studied in detail.

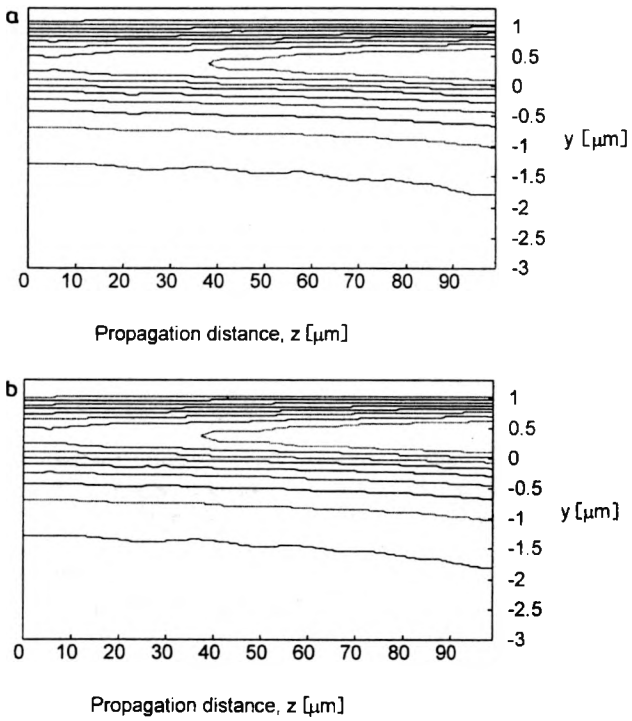

Fig. 2. Field intensity contour plots in the vertical cross-section $x=0$ for a 3D embossed rib waveguide taper operating at 1.15 μm with $w_i=1.5$ μm, $w_0=0.8$ μm, $n_f=3.44$, $n_s=3.4$, $n_c=1.0$, $L=100$ μm, $h=1$ μm: **a** — standard tapered FD BPM [4], [5], **b** — present tapered FD BPM with displaced boundary. The waveguide is between $y=0$ μm and $y=1$ μm. Contours are given at intervals of 0.1, starting from 0.05 of the maximum value.

To illustrate the field behaviour at the air-semiconductor of this typical structure we used the standard tapered FD BPM [4] to calculate the field intensity distribution for the vertical cross-section $x=0$ and present this in Fig. 2**a**. It is seen that there is little radiation into the air and the optical field is guided predominantly in the core and substrate, which confirms the validity of the assumption that the energy transported through the air-dielectric interface is negligible. In Figure 2**b** the corresponding field distribution calculated with the tapered FD BPM with the

displaced boundary is shown for comparison. Good overall agreement between these results is observed. It is also noted that numerical noise is not observable in the results obtained using either method so the tapered FD BPM with displaced boundaries maintains this desirable feature.

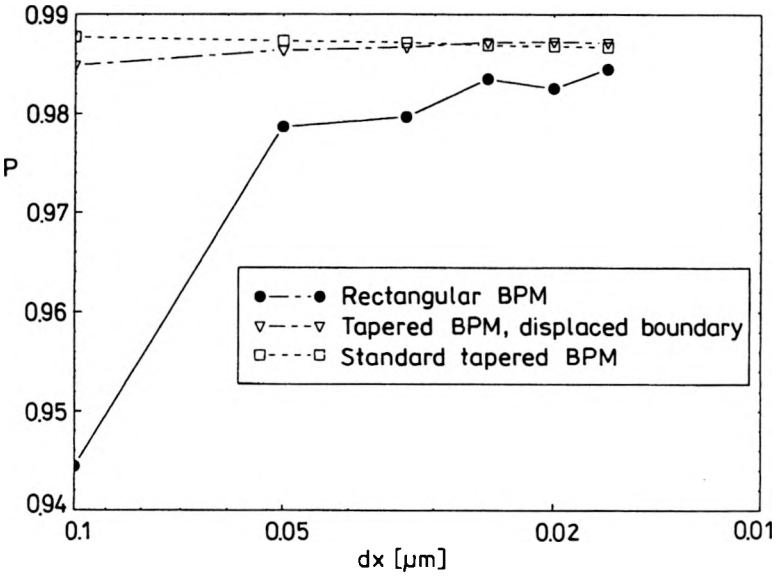

Fig. 3. Dependence of the power in the fundamental mode at the end of the structure analysed as a function of the transverse mesh size for a 3D embossed rib waveguide taper operating at 1.15 μm: $w_i = 1.5$ μm, $w_0 = 0.8$ μm, $n_f = 3.44$, $n_s = 3.4$, $n_c = 1.0$, $L = 100$ μm, $h =$ μm, $\Delta z = 0.1$ μm.

In Figure 3, the dependence of P, the power guided in the local fundamental mode at the end of the taper, is shown as a function of the transverse mesh size with Δz fixed at 0.1 μm. Three sets of results, produced by the tapered FD BPM algorithms with and without the displaced boundaries and a rectangular mesh FD BPM, are presented. All three methods converge to the same result, which once more confirms the validity of the assumptions made and the accuracy of the present method. It is also seen that the novel algorithm with displaced boundaries has the same fast convergence rate as the standard tapered algorithm. Results calculated using standard and displaced boundary FD BPM algorithms with a transverse mesh size of 0.02 μm and $\Delta z = 0.1$ μm for structures having $h = 0.3$, 0.5, 0.7 and 0.9 μm also showed agreement in P to at least 0.1%.

In the Table the time needed by each of the three algorithms on a Pentium 200 PC running Salford FORTRAN77 for the tapers with $h = 1$ μm and $h = 0.3$ μm is given as a function of the transverse mesh size. In the rectangular and standard taper BPM calculations a horizontal Hadley-type TBC [11] was positioned two Goos –Hänchen shifts above the top of the rib, the minimum distance found by numerical experiment to introduce an error in P of less than 1%, and the calculation window at the start of the taper was 12 μm (x direction) by 5 μm (y direction) for $h = 1$ μm

T a b l e. Computation time for 3D rib taper FD BPM analysis with $h = 1$ μm (embossed guide) and $h = 0.3$ μm, together with estimated computer memory needed for the embossed guide calculations. $w_i = 1.5$ μm, $w_0 = 0.8$ μm, $n_f = 3.44$, $n_s = 3.40$, $n_c = 1.0$, $L = 100$ μm, $\Delta z = 1$ μm.

dx = dy [μm]	CPU time [s] (computer memory [Mbyte])		
	displaced boundary tapered FD BPM	tapered FD BPM	rectangular FD BPM
Embossed guide ($h = 1$ μm)			
0.1	70 (1.5)	107 (1.9)	112 (1.9)
0.05	434 (6.2)	648 (7.8)	709 (7.8)
0.033	1342 (13.9)	2142 (17.5)	2455 (17.5)
$h = 0.3$ μm			
0.1	140 (2)	142 (2.1)	146 (2.1)
0.05	724 (8)	868 (8.5)	975 (8.5)
0.033	2122 (17.8)	2736 (19.2)	3151 (19.2)

and 14 μm × 5 μm for $h = 0.3$ μm. It is noted that in the case of FD BPM algorithm with displaced boundary there is no need to calculate the field intensity, and consequently store the respective field values in the computer memory, in the mesh nodes situated above the displaced boundary (*i.e.*, in the air region). To demonstrate the resulting benefits the table also shows the memory needed by each algorithm for the embossed case. It is seen that the novel algorithm is much faster than both the standard tapered FD BPM and the rectangular FD BPM. The explanation of this fact is that the tapered algorithm with displaced boundary benefits not only from the elimination of the numerical noise, as the standard tapered FD BPM, but also from the reduction in the number of mesh points in each cross-section. So, by introducing the displaced boundary we benefit in two ways, namely we shorten the calculation time and decrease the amount of the memory needed. We note also that the amount of time saved grows with the finer mesh resolution. Of course it is also possible to arrange for a TBC to follow the contour of the rib in the manner indicated in Fig. 1c. In this case our numerical calculations show that the TBC should be placed at least four Goos–Hänchen shifts away from the physical position of the semiconductor-air boundary otherwise accuracy is compromised. The present method, which places the $E = 0$ boundary only one Goos–Hänchen shift away from this boundary, always offers a better option.

4. Conclusions

We have demonstrated that a novel tapered BPM algorithm, which replaces semiconductor-air boundaries by displaced boundaries on which the zero field condition is set, provides a fast and accurate tool for the analysis of air clad optical waveguide tapers. The results obtained confirm that the new method is faster and

requires less memory than previous FD-BPM techniques, namely the tapered and rectangular FD BPM, and is as accurate as they are.

Acknowledgements – The authors thank the UK EPSRC for their support of this work under grant GR/L28753. Dr. Sujecki also thanks the Royal Society/Wolfson Foundation for the financial support of a Visting Fellowship.

References

[1] XU C.L., HUANG W.P., *Finite difference beam propagation method for guided wave optics*, [In] *Progress in Electromagnetics Research, Electromagnetic Waves, PIER 11*, [Ed.] W.P. Huang, EMW Publ., Cambridge, Ma, 1995, pp. 1–49.
[2] HAES J., *et al.* J. Light Technol. **14** (1996), 1557.
[3] SEWELL P., SUJECKI S., BENSON T.M., KENDALL P.C., *A Novel Beam Propagation Algorithm for Three Dimensional Optical Tapers*, Opt. Soc. Am., 1998, Technical Digest Series, Vol. 4, *Integrated Photonics Research*, pp. 14–16.
[4] SEWELL P., BENSON T.M., KENDALL P.C., ANADA T., Electron. Lett. **32** (1996), 1025.
[5] Sujecki S., SEWELL P., BENSON T.M., KENDALL P.C., To appear in IEEE J. Lightwave Technol.
[6] ADAMS M.J., *An Introduction to Optical Waveguides*, Wiley, Chichester, New York 1981.
[7] MATIN A., BENSON T.M., KENDALL P.C., STERN M.S., Int. J. Numer. Modelling: Electronic Networks, Devices and Fields **7** (1994), 25.
[8] KENDALL P.C., MCILROY P.W.A., STERN M.S., Electron. Lett. **25** (1989), 107.
[9] STERN M.S., XU C.L., MA F., HUANG W.P., *The Use of a Sparse Matrix Eigenmode Solver in Semivectorial Finite Difference Modelling of Optical Waveguides*, Opt. Soc. Am., 1995, Technical Digest Series, Vol. 7, *Integrated Photonics Research*, pp. 140–142.
[10] VAN DER VORST H.A., SIAM J. Sci. Statistics Comp. **13** (1992), 631.
[11] HADLEY R.G., Opt. Lett. **16** (1991), 624.

Received November 15, 1999